Integrated Optical Circuits

JAMES E. GOELL, MEMBER, IEEE, AND ROBERT D. STANDLEY, MEMBER, IEEE

Abstract—Research on optical communication systems indicates the future need for a compact, rugged, and economical medium for circuit realization. Encapsulated planar arrays of rectangular dielectric waveguides are attractive for this purpose. The individual guides would have dimensions on the order of a few micrometers while the planar arrays might cover an area of a few square centimeters. Integrated circuit technology appears adaptable to batch processing such circuits. Recent theoretical and experimental results are surveyed which support this viewpoint.

I. Introduction

THE realization of laser communication systems with enormous information capacity is envisioned. Regardless of the transmission medium, such systems may require extensive optical circuitry to process the communication signals. Toward this end consideration is being given to possible physical forms of the circuitry [1]. Natural objectives are compactness, environmental insensitivity, flexibility in performing signal processing functions, and economy.

Historically, the progression of electronic circuit development has been from a hybrid technology to a monolithic technology. The work surveyed in this paper suggests that optical circuitry may evolve along similar lines. At this juncture, a short-distance transmission medium is required which exhibits low loss over distances comparable to the circuit dimensions (a few centimeters) and lends itself to the fabrication of bends, couplers, filters, and other passive and active components required for optical signal processing.

A dielectric waveguide approach is very promising. Considerable information about such guides can be extracted from the fiber optics field where transmission losses below 0.01 dB/cm have been achieved. (The use of a metallic waveguide can be quickly eliminated since the loss of a waveguide having dimensions comparable to the wavelength would be on the order of 10^2 dB/cm.) Presently envisioned fabrication techniques make possible the realization of dielectric waveguides on dielectric substrates having approximately the cross sections of Fig. 1(a)–(c). In all cases the guided energy is concentrated in the core, i.e., the region of highest refractive index. Using such waveguides, directional couplers could be formed as shown in Fig. 1(d) and modulators as shown in Fig. 1(e). Various other active and passive circuits could also be realized [1].

II. Dielectric Waveguide Theory

In this section some of the pertinent theory of propagation in dielectric waveguide structures is given. First, we treat the slab case to give insight into general properties of dielectric waveguides. In addition, the theory is related to some useful thin-film measurement techniques to be discussed in Section III. Following this, propagation in rectangular dielectric waveguides is treated.

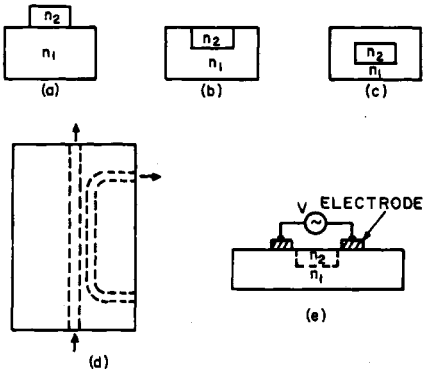

Fig. 1. Dielectric waveguide structures ($n_2 > n_1 \geq n_0$). (a) Raised guide. (b) Imbedded guide. (c) Encapsulated guide. (d) Directional coupler. (e) Modulator.

A. Slab Waveguide

The theory of propagation of electromagnetic waves in dielectric slabs is well documented in [2] and [3]. We state here the pertinent results without derivation. Consider the geometry of Fig. 2, where a lossless dielectric slab of thickness b and index of refraction n_1 is bounded by regions having indices n_2 and n_3 with $n_1 > n_2 \geq n_3$. The slab is assumed to be of infinite extent in the y direction. Both transverse electric (TE) and transverse magnetic (TM) modes of propagation are possible for this geometry.

It can be shown that the electric and magnetic fields vary as

$$(E, H) \alpha \begin{Bmatrix} \sin (k_x x) \\ \cos (k_x x) \end{Bmatrix} \exp (j(\omega t - \beta z)), \qquad |x| \leq b/2 \quad (1)$$

$$(E, H) \alpha \exp (\gamma_2 (x + b/2)) \exp (j(\omega t - \beta z)), \qquad x \leq -b/2 \quad (2)$$

and

$$(E, H) \alpha \exp (-\gamma_3 (x - b/2)) \exp (j(\omega t - \beta z)), \quad x \geq b/2. \quad (3)$$

The dispersion relations for the propagating modes are given by

$$\tan (k_x b) = \frac{\gamma_2/k_x + \gamma_3/k_x}{1 - (\gamma_2/k_x)(\gamma_3/k_x)} \quad (4)$$

for TE modes, and by

$$\tan (k_x b) = \frac{n_1^2(\gamma_2/n_2^2 + \gamma_3/n_3^2)}{1 - n_1^4 \gamma_2 \gamma_3/(n_2 n_3 k_x)^2} \quad (5)$$

for the TM modes, where the n's are the refractive indices

Manuscript received May 20, 1970.

The authors are with the Crawford Hill Laboratory, Bell Telephone Laboratories, Inc., Holmdel, N. J. 07733.

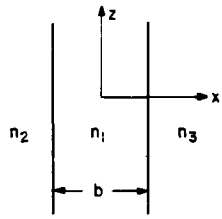

Fig. 2. Dielectric slab waveguide.

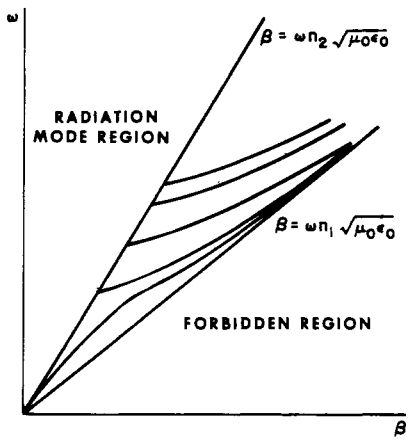

Fig. 3. ω versus β for a dielectric slab waveguide ($n_2 = n_3$).

of the various regions shown in Fig. 2, the γ's the exponential decay constants in the outer regions, and k_x the transverse propagation constant in the central region. These constants are related to each other and the longitudinal propagation constant β by the relations

$$\begin{aligned} \beta^2 &= k^2 n_2^2 + \gamma_2^2 \\ \beta^2 &= k^2 n_3^2 + \gamma_3^2 \\ \beta^2 &= k^2 n_1^2 - k_x^2 \end{aligned} \tag{6}$$

where

$$k = 2\pi/\lambda_0 = \omega\sqrt{\mu_0 \varepsilon_0}.$$

From the preceding relations the following necessary conditions for propagation can be derived

$$bk(n_1^2 - n_2^2)^{1/2} > \tan^{-1}\left[(n_2^2 - n_3^2)/(n_1^2 - n_2^2)\right]^{1/2} \tag{7}$$

for TE modes, and

$$bk(n_1^2 - n_2^2)^{1/2} > \tan^{-1}\left[n_1^4(n_2^2 - n_3^2)/n_3^4(n_1^2 - n_2^2)\right]^{1/2} \tag{8}$$

for TM modes.

A typical plot of ω versus β for the case $n_2 = n_3$ is given in Fig. 3 for TE or TM propagation. Also shown are the lines $\beta = \omega n_1\sqrt{\mu_0\varepsilon_0}$ and $\beta = \omega n_2\sqrt{\mu_0\varepsilon_0}$. All guided propagating wave solutions lie in the region between these boundaries. Unlike the case of the hollow metallic waveguide, a principal mode exists, that is, a mode that propagates at all frequencies. Also, for all other modes, propagation ceases at a nonzero β.

In the region to the left of the upper boundary, a continuum of radiating modes exist. The slope of the upper boundary is the velocity of light in the outer medium, and the slope of the lower boundary is the velocity of light in the core. For propagation near the lower boundary, the fields are confined mainly to the core. In the limit as the upper boundary is approached, the fields extend to infinity.

The ω versus β plots for $n_2 \neq n_3$ are similar to Fig. 3, except that a principal mode does not exist.

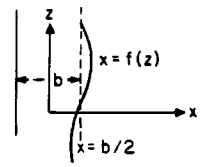

Fig. 4. Slab guide with wall imperfection.

B. Effects of Surface Imperfections

As stated previously, the rigorous solution of dielectric waveguide problems results in a discrete spectrum of guided modes plus a continuum of radiation modes. The effect of surface or bulk imperfections in a guide is to cause 1) coupling between a given guided mode and all propagating modes, and 2) coupling to the continuum of radiation modes. The latter results in increasing the waveguide loss above that due to dielectric absorption loss. Marcuse [4] has considered these effects for the dielectric slab waveguide shown in Fig. 4 with the simplifying assumption of no dimensional or other guide property variations in the y direction. Here we give only the results of his radiation loss calculations. Assuming that one wall is perfectly smooth and that for the other wall the imperfections have a sinusoidal shape of the form

$$f(z) - \frac{b}{2} = a \sin \phi z \tag{9}$$

then for $n_1/n_2 = 1.01$, $n_2 = n_3$, $n_2 b/\lambda = 4.78$, $\lambda_0 = 1$ μm, $4\pi/b\phi = 25$, and $n_2 L/\lambda_0 = 10^4$ where L is the guide length, it is found that the fractional power loss is

$$\frac{\Delta P}{P} = 0.1 \quad \text{for} \quad n_2 a/\lambda_0 = 0.0546.$$

Thus, for $n_2 = 1.5$, a 3.19-μm-thick slab guide with wall imperfections of 364 Å would result in a radiation loss of 0.69 dB/cm for a 1-μm wavelength.

For the case of random imperfections on one wall, Marcuse has considered the case where the correlation function of $f(z)$ is of the form

$$R(u) = A^2 \exp\left(-\frac{|u|}{B}\right) \tag{10}$$

where A is the root mean square deviation of the wall from perfect straightness, B is the correlation length, and $u = z - z'$. Fig. 5, taken from Marcuse, shows the normalized radiation loss for a guide of length L for the case $n_1 = 1.01$, while Fig. 6 gives the results for $n_1 = 1.5$. For both cases $n_2 = 1$. From these data, in a single mode waveguide, a deviation of the guide wall of about 3 percent for the worst case of correlation length results in a loss[1] of 0.5 dB/cm for an index

[1] It should be noted that the loss decreases with increasing correlation length for $2B/b$ sufficiently large so that a slow variation of the waveguide width is not serious. Furthermore, a few relatively large discontinuities could be tolerated.

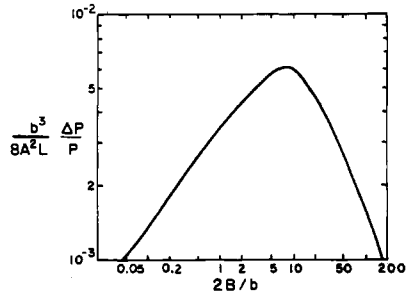

Fig. 5. Normalized radiation loss $(b^3/8A^2L)$ $(\Delta P/P)$ as a function of the normalized correlation length $2B/b$ for $n_1/n_2=1.01$, $kb=16.0$, and $n_2=1$. (Single guided mode operation.)

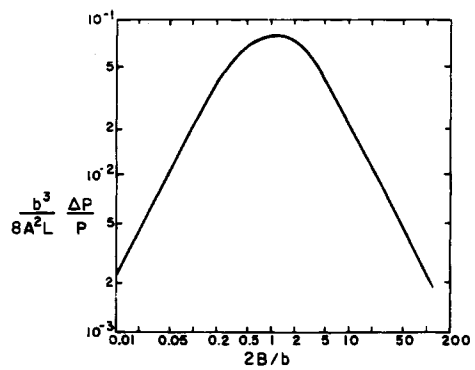

Fig. 6. Normalized radiation loss $(b^3/8A^2L)$ $(\Delta P/P)$ as a function of the normalized correlation length $2B/b$ for $n_1/n_2=1.5$, $kb=2.6$, and $n_2=1$. (Single guided mode operation.)

ratio of 1.01 and an outer index of 1.5. For an index ratio of 1.5 the loss is about an order of magnitude higher. For correlation functions other than (10), similar results are found for values of $2B/b$ less than that of the peak.[2]

C. Rectangular Dielectric Waveguide

The analysis of a rectangular dielectric waveguide is considerably more complex than that of the slab waveguide discussed in the preceding paragraphs. Unlike the previous case or that of the hollow metallic rectangular waveguide, the electric and magnetic fields of the rectangular dielectric waveguide modes cannot be expressed as functions exhibiting simple sinusoidal transverse variation in the core.

A number of methods have been employed to evaluate the properties of rectangular dielectric waveguide. Schlosser and Unger [5] have used a numerical approach employing sums of sine, cosine, and exponential functions. Their method is computationally best suited to cases of large aspect ratio (width to height) and to cases away from cutoff, that is, far from the radiation mode region. Marcatili [6] has obtained an approximate analytical solution in closed form also using simple sinusoidal and exponential functions. His solutions are accurate for the cases of small to moderate index difference and away from cutoff. Goell [7] has performed a numerical analysis employing cylindrical space harmonics. His solutions converge rapidly for aspect ratios between 1 and 2 and any index difference.

Fig. 7 shows the geometry used by Marcatili. In his

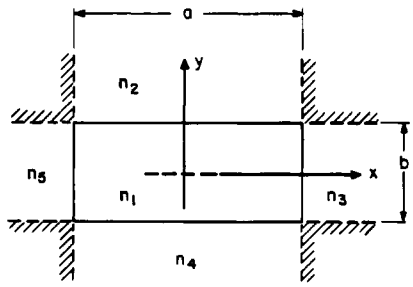

Fig. 7. Idealized rectangular waveguide geometry.

analysis the fields in the shaded regions are neglected which accounts for both the simplicity and limitations of his approach. For the case where most of the energy is confined to the core, he shows that the longitudinal propagation constant can be written as

$$\beta = (k_1^2 - k_x^2 - k_y^2)^{1/2} \tag{11}$$

where k_x and k_y are the x- and y-direction propagation constants in the core and are given by

$$k_x = \frac{\pi p}{a}\left(1 + \frac{A_3 + A_5}{\pi a}\right)^{-1} \tag{12}$$

$$k_y = \frac{\pi q}{a}\left(1 + \frac{n_2^2 A_2 + n_4^2 A_4}{\pi n_1^2 b}\right)^{-1} \tag{13}$$

for E_{pq}^y modes, and by

$$k_x = \frac{\pi p}{a}\left(1 + \frac{n_3^2 A_3 + n_5^2 A_5}{\pi n_1^2 a}\right)^{-1} \tag{14}$$

$$k_y = \frac{\pi q}{a}\left(1 + \frac{A_2 + A_4}{\pi b}\right)^{-1} \tag{15}$$

for E_{pq}^x modes, where

$$A_m = \frac{\pi}{(k_1^2 - k_m^2)^{1/2}} = \frac{\lambda}{2(n_1^2 - n_m^2)^{1/2}} \tag{16}$$

and

$$k_m = \frac{2\pi}{\lambda_m} = \omega\sqrt{\mu_0 \varepsilon_m}. \tag{17}$$

In these equations, p and q represent the number of field maxima in the x and y directions, respectively, m the region number as defined in Fig. 7, and the superscripts x and y give the polarization of the principal component of the electric field.

Fig. 8 shows some typical curves of normalized propagation constant $\mathcal{P}^2=(k_z^2-k_4^2)/(k_1^2-k_4^2)$ versus normalized waveguide height $\mathcal{B}=b/\lambda_0(n_1^2-n_4^2)^{\frac{1}{2}}$. Included are curves drawn using (11) and (12), curves found from more accurate transcendental relations also derived by Marcatili, and curves derived numerically by Goell. The divergence of the curves near cutoff is due to approximations imposed by Marcatili. Curves of the principal mode propagation constants for unit aspect ratio are shown in Fig. 9 for several values of $\Delta n_r=n_1/n_4-1$. The curves are relatively insensitive to the index difference due to the normalization employed to define the coordinates.

[2] D. Marcuse, private communication.

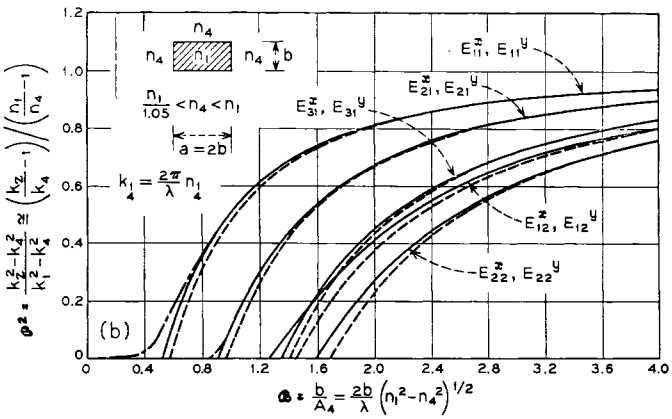

Fig. 8. Propagation constant for several modes of rectangular waveguide [6]. —— transcendental equation solution; – – – closed form solutions; – · – · – Goell's computer solutions.

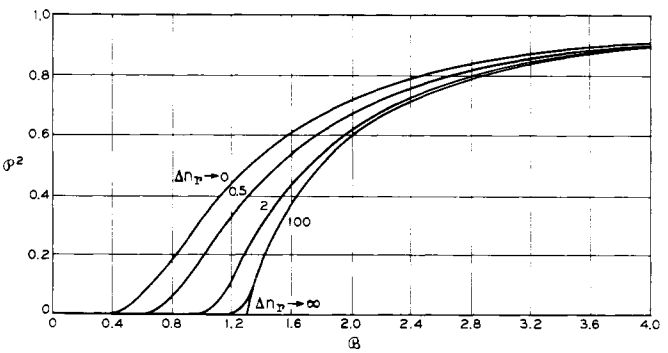

Fig. 9. Effect of index difference Δn on β [7] for unity aspect ratio.

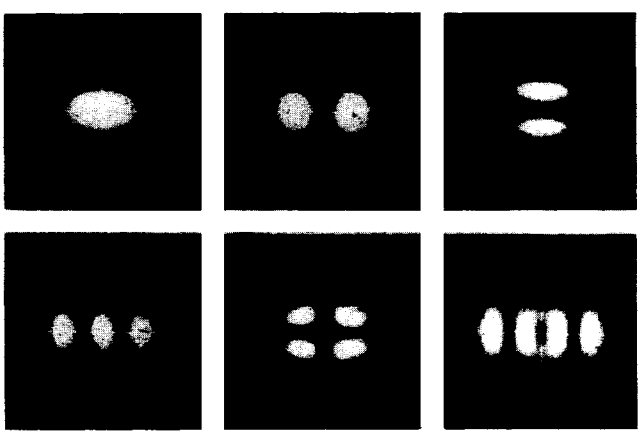

Fig. 10. Computer images of E_{pq}^y modes with $a/b = 2$, $\mathcal{B} = 2$, and $\Delta n_r = 0.01$. (a) E_{11}^y. (b) E_{21}^y. (c) E_{12}^y. (d) E_{31}^y. (e) E_{22}^y. (f) E_{41}^y [7].

Computer generated images of the first six rectangular dielectric waveguide modes are shown in Fig. 10 for a normalized guide height of 2. These images were obtained by generating dots whose area was proportional to the calculated local mode power density. The outlined rectangle represents the core boundary. Even for the E_{41}^y mode, where the normalized propagation constant is 0.12, most of the power is confined to the core and very little exists in the shaded region of Fig. 7. This accounts for the accuracy of Marcatili's analysis even for fairly small values of normalized propagation constant. Fig. 11 demonstrates the extension of the fields outside the core region as cutoff is approached. Similar results are obtained for all modes.

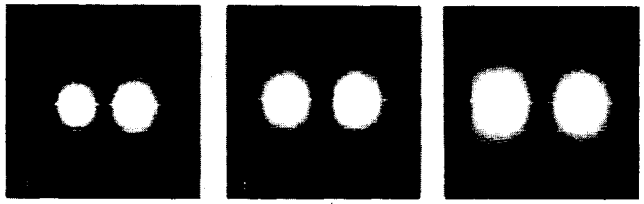

Fig. 11. Power density as cutoff is approached. Computer images of the E_{21}^y mode. (a) $\mathcal{P}^2 = 0.76$. (b) $\mathcal{P}^2 = 0.31$. (c) $\mathcal{P}^2 = 0.04$ [7].

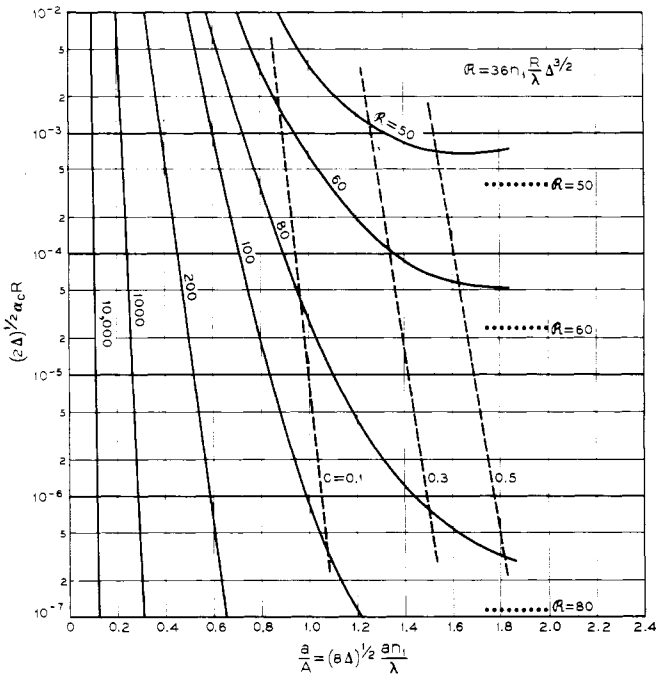

Fig. 12. Attenuation per radian for E_{11}^x and E_{11}^y modes if $n_1/n_3 = 1 + \Delta$ and $\Delta \ll 1$ [8].

D. Bends

Practical circuit realization will require dielectric waveguide bends. The ability of such waveguides to negotiate bends and the radiation loss thus produced have been considered by Marcatili [8]. Fig. 12 shows normalized loss data for a typical range of parameters. Here α_c is the attenuation coefficient of the waveguide bend, and R is the radius of curvature of the bend. The parameter c is given by

$$c = \frac{a^2\beta^2}{4k_x R} \tag{18}$$

where β is the longitudinal propagation constant of a straight waveguide and the transverse propagation constant k_x is given by (12) for the E_{pq}^y modes or by (14) for the E_{pq}^x modes. The parameter A in the ordinate dimension is

$$A = \frac{\lambda_0}{2(n_1^2 - n_3^2)^{\frac{1}{2}}}. \tag{19}$$

The solid lines in Fig. 12 are accurate to the left of the dashed line given by $c = 0.3$. For large c the dotted curves apply.

For an example of the loss expected, consider

$$n_1 = 1.5$$

$$a = \frac{\lambda_0}{2n_1\left(1 - \frac{n_3^2}{n_1^2}\right)^{\frac{1}{2}}} \quad \text{(single mode guide)}$$

then a 1-percent attenuation (0.087 dB) resulting from radiation in a length of guide equal to R is achieved with the values shown in Table I. The smaller $n_1 - n_3$, the larger the radius of curvature. For $\lambda_0 = 0.63$ μm, if one wants to keep R below 1 mm, the difference between the internal and external refractive indices must be larger than 0.01. Table I applies to the case $b = \infty$. For finite b the value of R must be multiplied by $[1-(k_y/k_3)^2]^{-1}$.

TABLE I

$1-(n_3/n_1)$	a/λ_0	R/λ_0
0.1	0.745	30
0.01	2.36	1060
0.001	7.45	37000

E. Directional Couplers

Directional couplers will form an integral part of many integrated optical circuits. Typical results of Marcatili's analysis [6] on coupling of rectangular dielectric waveguides are shown in Figs. 13 and 14. The parameters not defined in these figures are the following,

$$K = \frac{\pi}{2L} = 2\frac{k_x^2}{k_z}\frac{\xi}{a}\frac{\exp(-c/\xi)}{1 + k_x^2\xi^2} \tag{20}$$

$$\xi = \left[\frac{1}{\left(\frac{\pi}{A_5}\right)^2 - k_x^2}\right]^{1/2} \tag{21}$$

where c is waveguide spacing and L is the length of the coupling region which results in complete power transfer from one guide to the other.

The coupled power is given by

$$P = P_0 \sin^2 Kl \tag{22}$$

where l is the length of the coupling region and P_0 the input power. We give two examples obtained from the above data. For

$$\left.\begin{aligned} n_1 &= 1.5 \\ n_2 &= 1.5/1.01 \\ b &= 1.77\,\lambda_0 \\ a &= 3.54\,\lambda_0 \end{aligned}\right\} \quad \text{(single mode guides)}$$

then for an interguide spacing equal to the waveguide width, complete transfer of power will occur in a length of 6540 λ_0. For one fourth of this separation, the interaction length for complete coupling will be 262 λ_0.

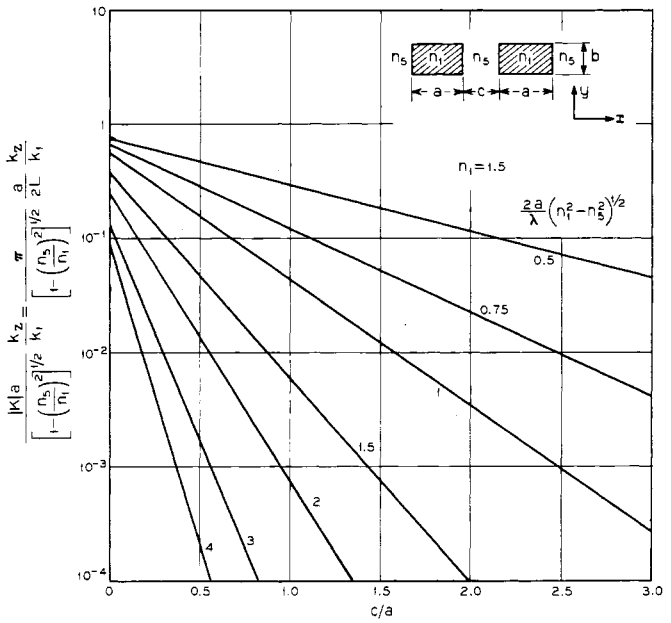

Fig. 13. Coupling coefficient for E_{1q}^x modes [6].

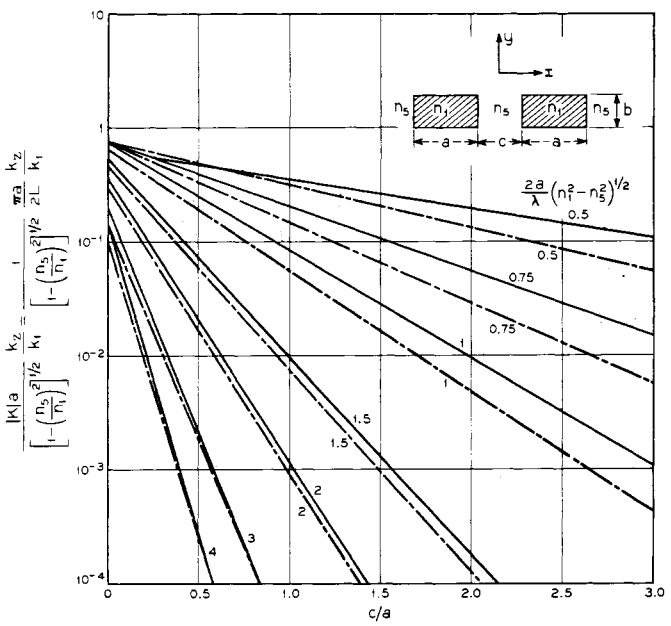

Fig. 14. Coupling coefficient for E_{1q}^x modes for $n_1/n_5 = 1.5$; ----E_{1q}^x coupling for $n_1/n_5 = 1.1$ [6].

III. Measurement of Optical Parameters

The measurement of the optical parameters of thin films has received considerable attention in the literature over a period of many years. For a thorough review of the field, the reader is referred to Heavens [9] and Abeles [10]. Our attention will be directed toward those techniques which have proven most suitable for our work. In particular, we shall treat Abeles' method of measuring the refractive index by determining the Brewster angle of a film. The effect of a graded index on the accuracy of this method will also be discussed. A more recent method of measurement using a prism to excite propagating modes in a film will also be described as will methods of measuring attenuation.

A. Analysis of Abeles' Method

When light polarized in the plane of incidence is incident on the air–film interface at the Brewster angle for the film, there is no reflection from the interface, i.e., the film behaves as if it did not exist. The reflected signal is then equal in magnitude to that which would be obtained from the substrate alone. More precisely, the reflection coefficient from a film of thickness d and index n_f on an infinitely thick substrate of index n_s is given by

$$R = \frac{r_f + r_s e^{-j2\delta}}{1 + r_f r_s e^{-j2\delta}} \tag{23}$$

where r_f and r_s are Fresnel coefficients, i.e.,

$$r_f = \frac{\cos \Phi_f - n_f \cos \Phi_i}{\cos \Phi_f + n_f \cos \Phi_i} \tag{24}$$

$$r_s = \frac{n_f \cos \Phi_s - n_s \cos \Phi_f}{n_f \cos \Phi_s + n_s \cos \Phi_f} \tag{25}$$

and

$$\delta = \frac{2\pi n_f d}{\lambda_0} \cos \Phi_f \tag{26}$$

where Φ_i is the angle of incidence in air; Φ_f is the angle of refraction in the film; and Φ_s is the angle of refraction in the substrate. At the Brewster angle, Φ_{iB} for the air–film boundary, $r_f = 0$, so that

$$\tan \Phi_{iB} = n_f. \tag{27}$$

We then obtain from above

$$|R| = \frac{\cos \Phi_s - n_s \cos \Phi_i}{\cos \Phi_s + n_s \cos \Phi_i} = r_{s0} \tag{28}$$

where r_{s0} is the Fresnel coefficient for the air-substrate boundary.

It can be shown that if $r_s = 0$, then $|r_f| = |r_{s0}|$ is also a solution. However, this root exists only in a restricted range of n_f and n_s given by

$$\frac{n_f^2 n_s^2}{n_f^2 + n_s^2} \leq 1. \tag{29}$$

Fig. 15 is a plot of the region for which this latter solution applies. In general, our work on silicate glass is in the region n_f, $n_s > 1.45$, so that this latter solution is of no concern. However, it could be significant in the evaluation of fluoride glass and other smaller index systems. In practice, the refractive index of a film can be determined to an accuracy better than ± 0.002 by this method.

B. Effect of Index Gradient

The Method described in the preceding paragraphs assumes that the film index is uniform. It is well known that for some materials, such as MgF_2, the refractive index varies with depth [11]. In order to gain insight into the effects of index gradients, consider the index profile of Fig. 16. For a transition region thickness $\Delta t = 0$, the analysis of Section III-A applies, so the true film index results from the measurement. However, for Δt finite an error will result, i.e., the measured index, $\bar{n}$ will not be n_f. Assuming that the transition from n_f to n_s is continuous, then for Δt sufficiently large it can be shown analytically that for n_f and n_s large or for $n_f \approx n_s$, the measurement described above gives the geometric mean of the film and substrate indices.

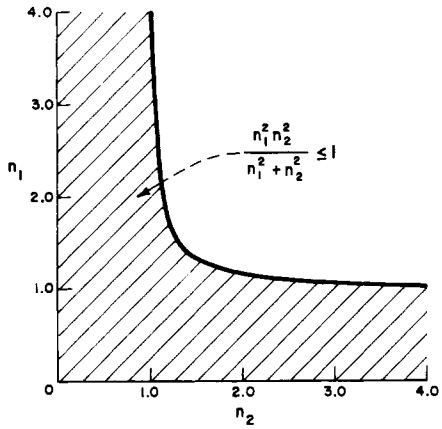

Fig. 15. Domain of substrate Brewster angle root.

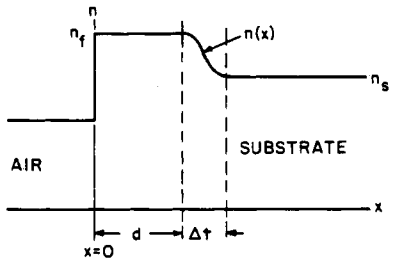

Fig. 16. Index gradient profile.

In order to obtain further information, a numerical analysis of the problem has been performed. It was assumed that $n(x)$, the index variation in the transition region, took the form

$$n(x) = \frac{n_f + n_s}{2} - \frac{n_f - n_s}{2} \cos\left(\frac{x - d}{\Delta t}\pi\right), \quad \text{for } d \leq x \leq d + \Delta t. \tag{30}$$

The problem was solved by using a matrix formulation with $n(x)$ approximated by a series of discrete steps [12]. Fig. 17 shows the variation of the measured index $\bar{n}$ as found by Abeles' method as a function of transition region thickness for a substrate index of 1.50 and a film thickness $d = 0.1\ \lambda_0$.

For a graded index, the measured index $\bar{n}$ is also a function of film thickness because the angle at which the reflection coefficient of the film on the substrate is equal to the reflection coefficient of the substrate alone is not equal to the Brewster angle for the film alone. This effect is demonstrated in Fig. 18. Clearly, even fairly short graded regions can cause significant error.

C. Film Loss Measurement

In order to determine the loss of films suitable for fabrication of waveguides, it is necessary that light be propagated in the film. Efficient injection of light by edge illumination is impractical since the films are typically about 0.3 μm thick. It has been found convenient to launch from a higher index region. One such method has been described by

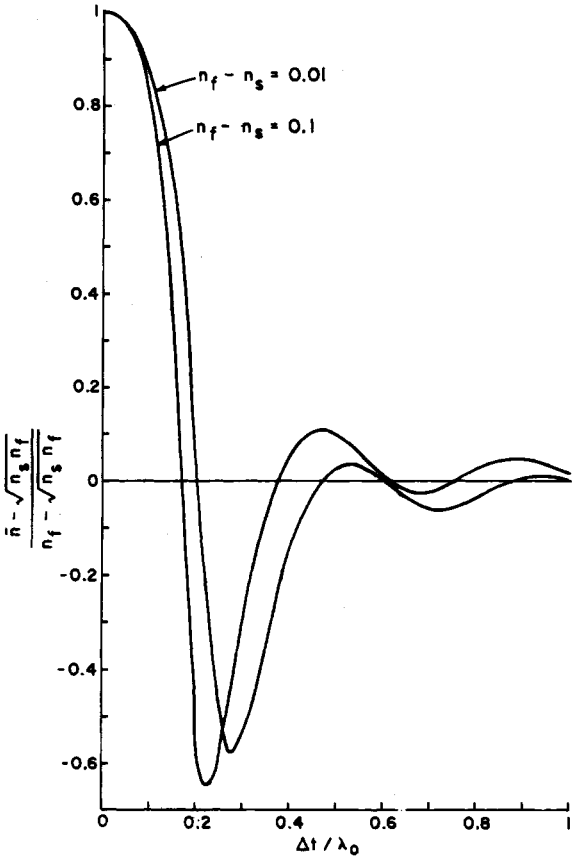

Fig. 17. Measured refractive index versus graded region thickness for $n_s = 1.5$, $d/\lambda_0 = 0.1$.

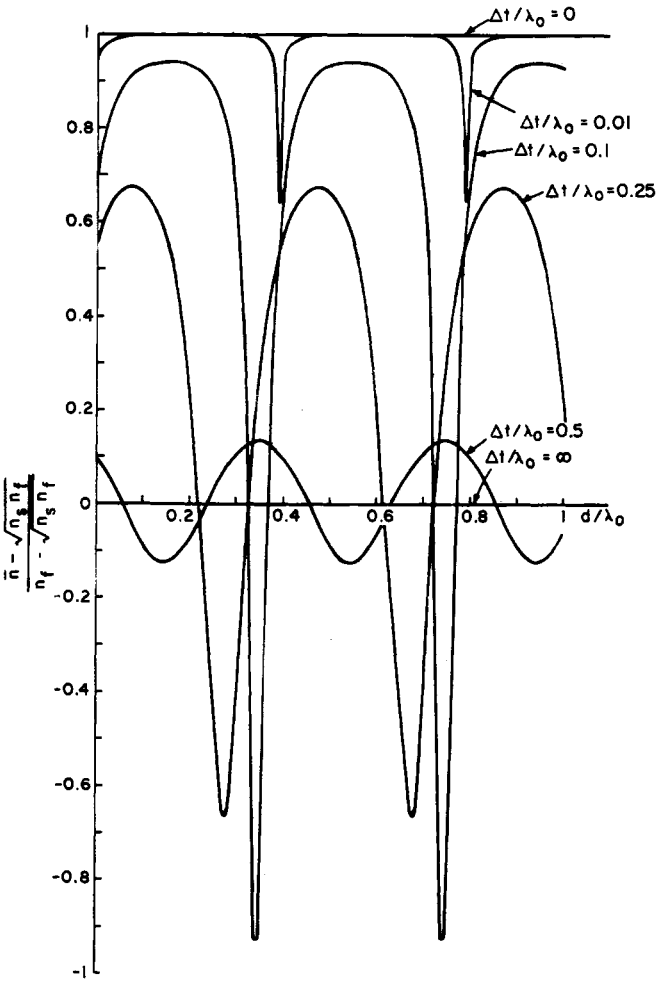

Fig. 18. Measured refractive index versus film thickness for $n_s = 1.5$, $n_f = 1.51$.

Osterberg and Smith [13]. Recently Tien, Ulrich, and Martin [14] have analyzed evanescent coupling via a higher index region. These latter results have been extended by Midwinter [15] to indicate the effects of strong coupling and finite beam size.

Referring to Fig. 19, a high index prism ($n_p > n_f$) is clamped to the film. By proper selection of the injection angle in the high index medium, the propagation constant of the incident beam can be made equal to that of the mode in the film. Assuming weak coupling, the incident angle of the input beam is related to the propagation constant of the film by

$$\phi = \sin^{-1}\left\{\frac{n_p}{n_0}\sin\left(\sin^{-1}\left(\frac{\beta}{k_0 n_p}\right) - \theta_c\right)\right\} \qquad (31)$$

where n_p is the prism refractive index; β is the mode propagation constant in film [see (1)–(5)]; θ_c is the corner angle of the prism (see Fig. 19); $k_0 = 2\pi/\lambda_0$; and ϕ is the angle of incidence of light with respect to the normal to the input face of the prism.

This relationship permits calculation of several important properties. For example, knowledge of ϕ, n_p, and θ_c permits calculation of β, which in turn allows determination of n_f or d. If several modes can be launched, the correlation of the various β's with n_f and d allows determination of both parameters. Another example is that (31) permits optimization of launching efficiency of modes by selecting θ_c so that ϕ is a Brewster angle.

In our work, 45-degree isosceles prisms fabricated from SF-58 Shott glass having an index of 1.9176 were used. To

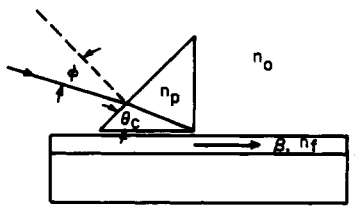

Fig. 19. Prism coupler.

date we have not attempted to maximize launching efficiency.

Several methods have been used to measure transmission loss [16]. The simplest approach is to photograph the scattered light from the film. Taking exposures of various durations, it is possible to estimate the film attenuation. A second method is to vary the position of the launching prism and measure either the power reaching the edge of the film or the intensity of light coupled from the film by a second prism. However, our experience has been that the variability of launching efficiency makes accurate determination of film loss difficult (to an accuracy of better than ± 2 dB).

The best accuracy has been achieved by measuring the intensity of light scattered at right angles to the film using a fiber optic probe. If the scattering centers are uniformly

dispersed in the film, then a plot of scattered power versus distance from the launcher permits determination of film loss. In our measurements the input beam is mechanically chopped at a 1-kHz rate. A silicon solar cell attached to the end of the fiber probe provides a signal whose strength is measured using a lock-in amplifier.

IV. Film and Waveguide Fabrication

Considerable effort is being directed toward the practical realization of optical integrated circuits. This work can be divided into two areas. First, a transparent thin-film medium must be found (< 1 dB/cm loss). Second, masking and etching techniques must be found which are suitable for use with the selected medium. From Marcuse's results (Section II-B), it appears that these techniques must be capable of generating an edge whose roughness is less than 0.1 λ_0. However, occasional discontinuities of much greater magnitude are tolerable.

A. Thin-Film Media

A number of techniques for producing thin films suitable for integrated optics application have been proposed. These include ion bombardment of fused quartz, ion exchange in glass, RF and dc sputtering, thermal evaporation, pyrolytic deposition, and epitaxy. The applicability of liquids and polymers is also being considered. We briefly review the results achieved by the methods which have shown the most promise to date.

1) Film Formation by Ion Bombardment: High refractive index regions have been created in fused silica by ion bombardment. Schineller *et al.* [17] achieved a 0.01 increase in refractive index using 1.5 MeV protons at a dosage of 10^{17} protons per cm. They demonstrated mode propagation in a 4-μm-thick irradiated region. The properties of waveguides made from these surface films have not been determined.

2) Ion Exchange: Osterberg and Smith [13] appear to be the first to have investigated the propagation of surface waves in graded index films produced by a diffusion technique in glass. In their experiments Pilkington Float glass, made by floating molten glass on molten tin, was used. The refractive index of the surface layer of the glass produced by this process is higher than the bulk. However, the surface layer was too thick (0.12 mm) for a single mode waveguide.

Other authors have described the use of ion exchange with glass fibers to produce a low index cladding [18], [19]. Efforts to produce suitable guiding regions in a planar geometry are in progress.

3) Sputtered Glass Films: RF sputtering of glass has been shown to be a very promising method of producing films suitable for optical waveguide [16]. Guidance in this type media has been demonstrated with a loss below 1 dB/cm.

The best films that have been prepared by this method used ordinary laboratory slides as substrates and Corning 7059 glass as the source material for the film. The refractive index of these films is 1.62 and that of the substrates 1.515. Other materials have also shown promise. Alumina-doped SiO_2 films have been produced whose quality approached that of the 7059 glass films and, with further work, may well surpass it. This system is particularly attractive because adjustment of the doping level allows continuous variation of the film index from 1.458 to about 1.6. However, early tests indicate that the higher index films have higher scattering loss and a lower sputtering rate than the lower index films, so it is the lower end of the index range which will probably be of most interest.

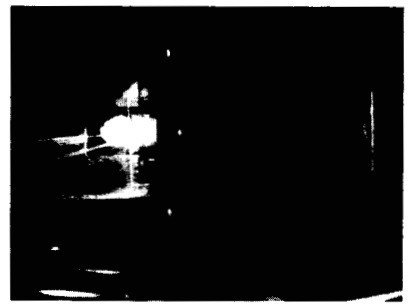

Fig. 20. Light scattered from a beam propagating in a Corning 7059 glass film [16].

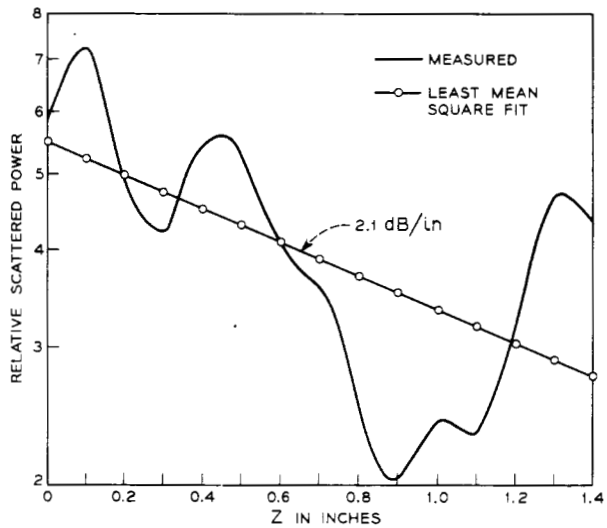

Fig. 21. Relative scattered power versus length (7059 glass film) [16].

Fig. 20 is a picture of the 0.6328-μm light scattered from a beam propagating in the film. The intensity of scattered light as measured by the fiber optic probe is plotted in Fig. 21. The measured loss is less than 1 dB/cm. This result is in agreement with photographic and two-prism measurements. The lack of uniformity of the scattered light intensity is due, at least in part, to inhomogeneities in the substrate. By using a higher quality substrate this source of scatter can be eliminated.

Curved sections of rectangular waveguides have been constructed from 7059 glass films by back-sputtering using quartz fibers as shadow masks. The waveguides were about 0.3 μm thick, 20 μm wide, and had a radius of curvature of about $\frac{1}{2}$ inch. A photograph of a typical section is shown in Fig. 22. Fig. 23 shows prism-launched light propagating in such a waveguide. Due to the small size of the waveguide our instrumentation will have to be improved before loss measurements can be made.

These results demonstrate the feasibility of using sputtered glass films and sputter etching in the fabrication of optical waveguides. The approach shows promise as a method of producing low-loss optical integrated circuits.

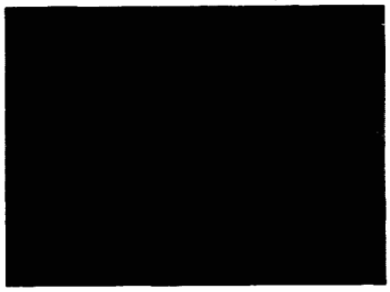

Fig. 22. Section of a rectangular waveguide (× 1000) [16].

Fig. 23. Light propagating in a curved section of rectangular waveguide [16].

B. Waveguide Fabrication

In Section II-B the edge roughness requirements were shown to be very stringent. Those computations indicate that the guide surfaces must be smooth to about 0.1 λ_0 in order that radiation loss be small. This imposes strict requirements on fabrication procedures. Conventional photolithographic techniques using optically exposed photoresist do not approach this order of edge resolution. Chemical etching of glass films usually results in clouding of the surface due to leaching of constituents, so etching by this method does not appear feasible. Hence, alternate fabrication methods are being pursued.

A promising approach is the use of a scanning electron beam to expose photoresist followed by reverse sputtering of the unwanted film. Other workers have reported exceptionally high-quality metal masks using electron-beam photoresist exposure. Gold grids consisting of 700-Å lines separated by 1400 Å have been produced [20] so that the required resolution appears achievable. Problems with this method of guide fabrication are photoresist-film compatibility, and the requirement that the resist withstand the temperature rise involved in back-sputtering. An additional problem involves the relatively slow writing times for circuits of the size we are considering using conventional scanning electron beam microscopes. By a stepping process involving mechanical movement of the substrate it should be possible to generate masks suitable for circuit fabrication.

V. Conclusions

Integrated optical circuits in the form of planar arrays of rectangular dielectric waveguides appear attractive for optical signal processing circuitry. We have summarized those aspects of the problem necessary for a basic evaluation of the approach. The problem of practical realization of such circuits appears solvable by appropriate adaptation of integrated circuit fabrication techniques. It has been shown that thin films suitable for planar dielectric waveguide applications can be produced by RF sputtering of glass. Other approaches also show promise. The problem of masking by a technique suitable for batch fabrication appears tractable, but further work is required in this area.

Acknowledgment

The authors wish to thank W. R. Sinclair for his valuable comments regarding the sputtering of glass films and the preparation of substrates, R. R. Murray who assisted in the preparation of our films and waveguides, and Miss R. E. Quinn for her aid in programming the index gradient problem.

References

[1] S. E. Miller, "Integrated optics: an introduction," *Bell Syst. Tech. J.*, vol. 48, pp. 2059–2069, September 1969.
[2] R. E. Collin, *Field Theory of Guided Waves*. New York: McGraw-Hill, 1960.
[3] D. F. Nelson and J. McKenna, "Electromagnetic modes of anisotropic dielectric waveguides at p-n junctions," *J. Appl. Phys.*, vol. 38, pp. 4057–4073, September 1957.
[4] D. Marcuse, "Mode conversion caused by surface imperfections of a dielectric slab waveguide," *Bell Syst. Tech. J.*, vol. 48, pp. 3187–3217, December 1969.
[5] W. Schlosser and H. G. Unger, "Partially filled waveguides and surface waveguides of rectangular cross section," in *Advances in Microwaves*. New York: Academic Press, Inc., pp. 319–387, 1966.
[6] E. A. J. Marcatili, "Dielectric waveguide and directional coupler for integrated optics," *Bell Syst. Tech. J.*, vol. 48, pp. 2071–2102, September 1969.
[7] J. E. Goell, "A circular-harmonic computer analysis of rectangular dielectric waveguides," *Bell Syst. Tech. J.*, vol. 48, pp. 2133–2160, September 1969.
[8] E. A. J. Marcatili, "Bends in optical dielectric guides," *Bell Syst. Tech. J.*, vol. 48, pp. 2103–2132, September 1969.
[9] O. S. Heavens, *Optical Properties of Thin Solid Films*. New York: Academic Press, Inc., 1955.
[10] F. A. Abeles, "Optics of thin films," in *Advanced Optical Techniques*. New York: Wiley, 1967, pp. 143–188.
[11] K. Nagota, "Inhomogeneity in refractive index of evaporated Mg F_2 film," *Japan J. Appl. Phys.*, vol. 7, pp. 1181–1185, October 1968.
[12] J. E. Goell and R. D. Standley, to be published.
[13] H. Osterberg and L. W. Smith, "Transmission of optical energy along surfaces: pt. II, inhomogeneous media," *J. Opt. Soc. Am.*, vol. 54, pp. 1078–1084, September 1964.
[14] P. K. Tien, R. Ulrich, and R. J. Martin, "Modes of propagating light waves in thin deposited semiconductor films," *Appl. Phys. Lett.*, vol. 14, pp. 291–294, May 1, 1969.
[15] J. E. Midwinter, "Evanscent field coupling into a thin film waveguide," to be published.
[16] J. E. Goell and R. D. Standley, "Sputtered glass waveguide for integrated optical circuits," *Bell Syst. Tech. J.*, vol. 48, pp. 3445–3448, December 1969.
[17] E. R. Schineller, R. Flam, and D. Wilmot, "Optical waveguides formed by proton irradiation of fused silica," *J. Opt. Soc. Am.*, vol. 58, pp. 1171–1176, September 1968.
[18] A. D. Pearson, W. G. French, and E. G. Rawson, "Propagation of a light focusing glass rod by ion-exchange techniques," *Appl. Phys. Lett.*, vol. 15, p. 76, 1969.
[19] T. Uchida, M. Furukawa, I. Kitano, K. Koizumi, and H. Matsumora, "A light-focusing fiber guide," presented at the 1969 IEEE Conf. on Laser Engineering and Applications, Washington, D. C., paper 7.7.
[20] A. N. Broers, "Combined electron and ion beam processes for microelectronics," *Microelectron. Rel.*, vol. 4, pp. 103–104, 1965.

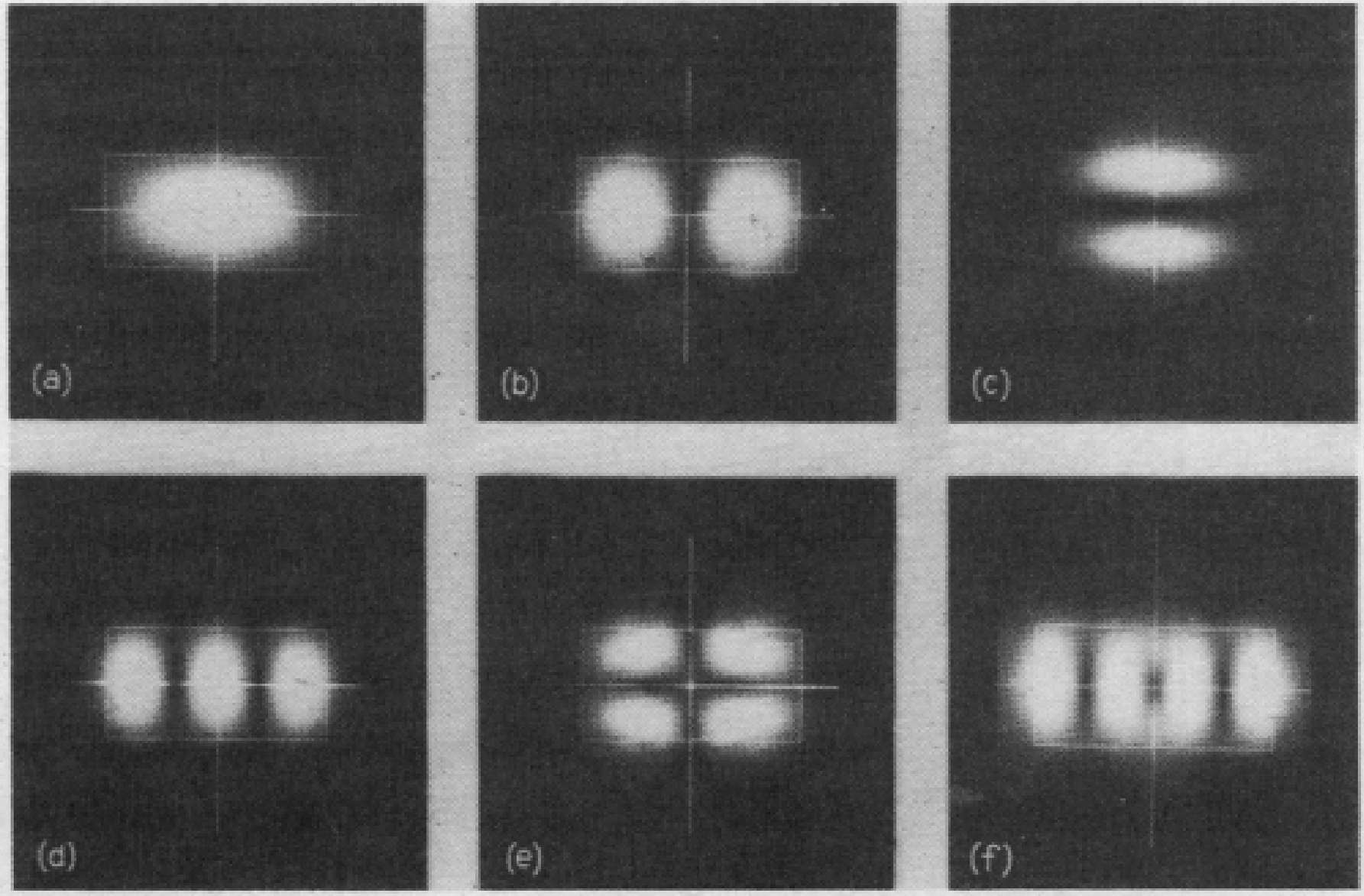

Fig. 10. Computer images of E^y_{pq} modes with $a/b = 2$, $\mathcal{R} = 2$, and $\Delta n_r = 0.01$: (a) E^y_{11}. (b) E^y_{21}. (c) E^y_{12}. (d) E^y_{31}. (e) E^y_{22}. (f) E^y_{41} [7].

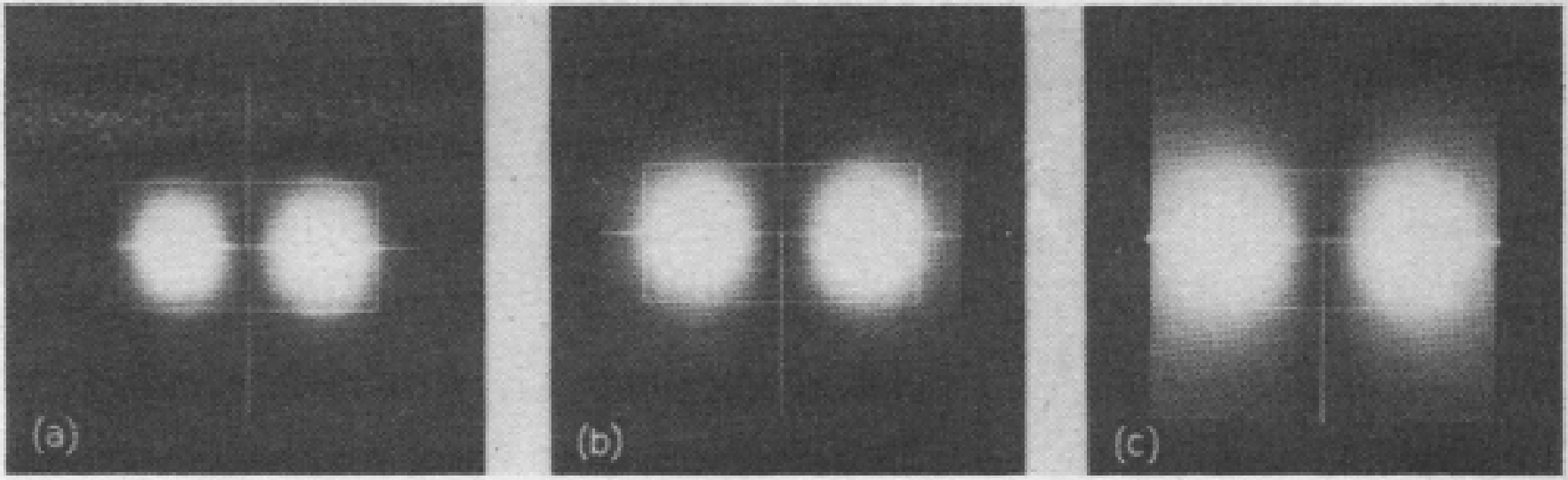

Fig. 11. Power density as cutoff is approached. Computer images of the E_y mode. (a) $\mathscr{P}^2 = 0.76$. (b) $\mathscr{P}^2 = 0.31$. (c) $\mathscr{P}^2 = 0.04$ [7].

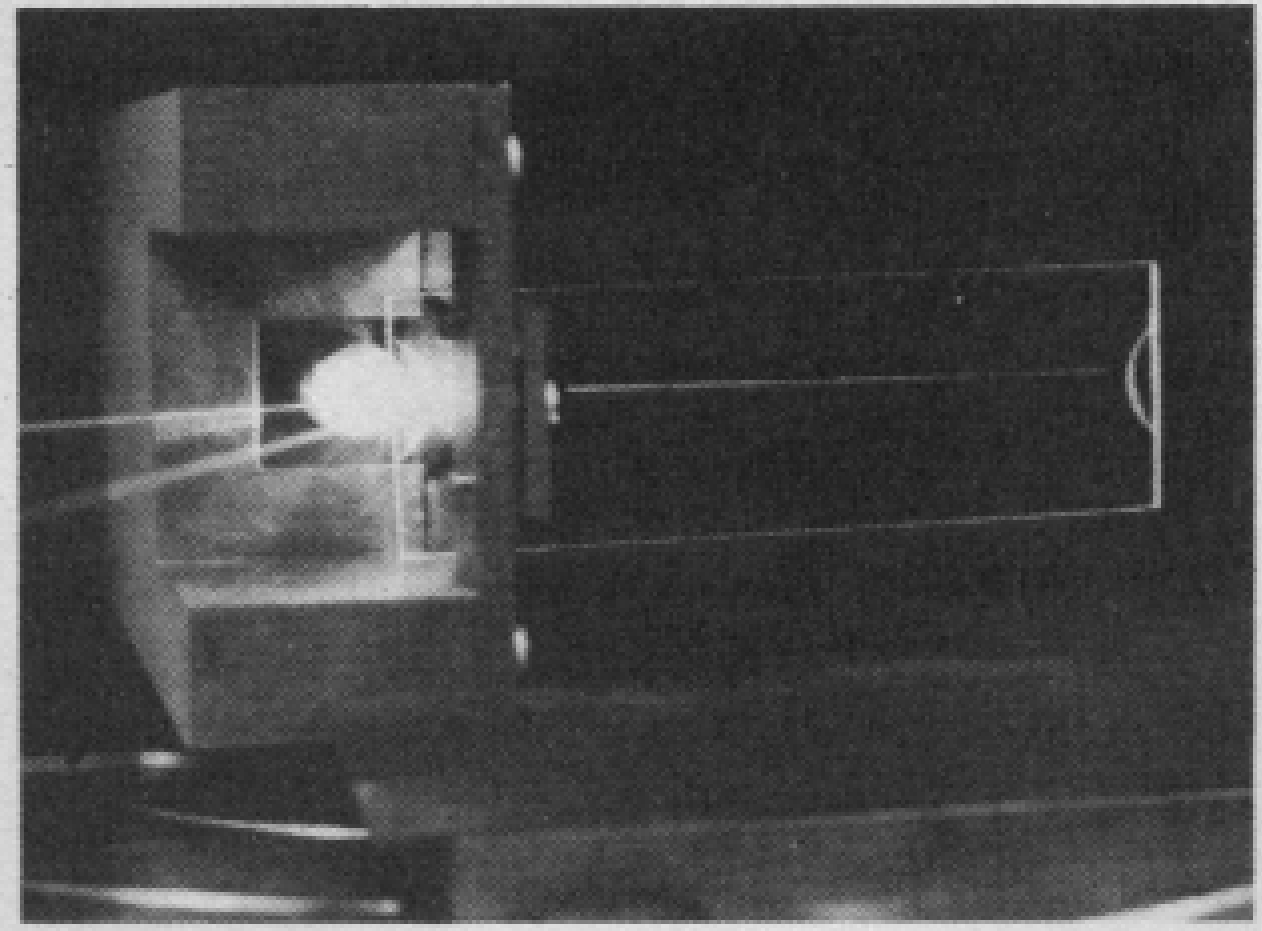

Fig. 20. Light scattered from a beam propagating in a Corning 7059 glass film [16].

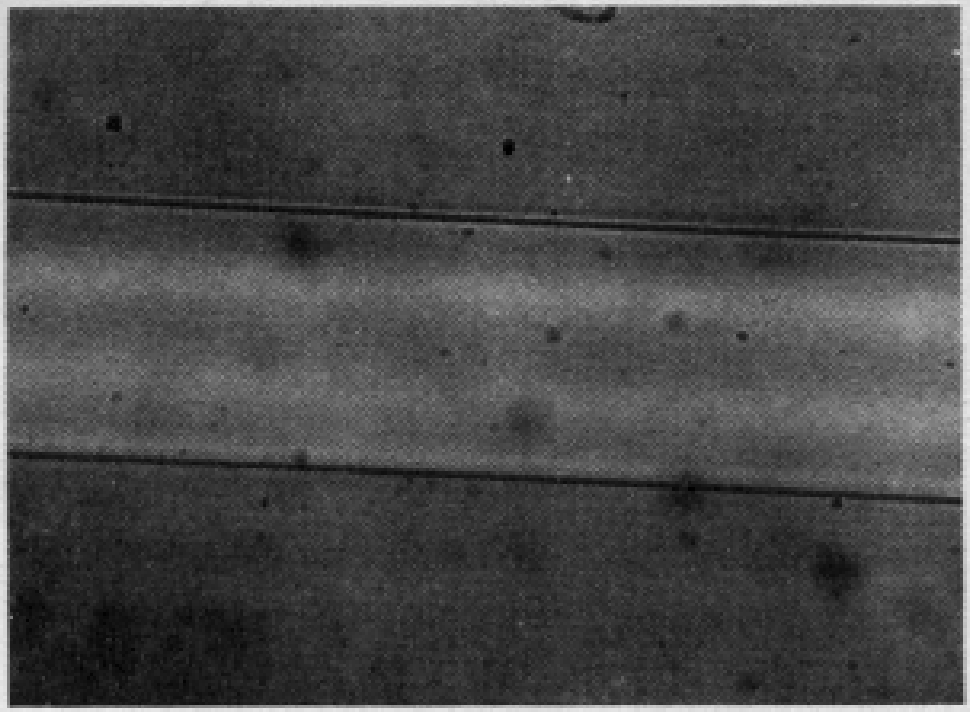

Fig. 22. Section of a rectangular waveguide (× 1000) [16].

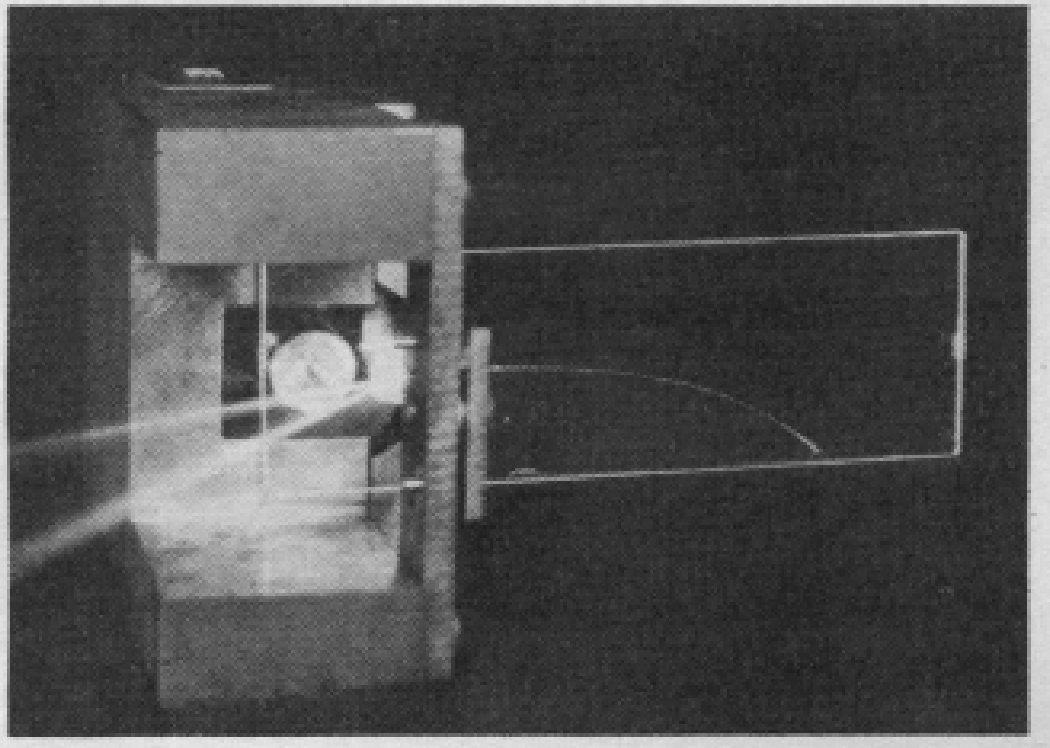

Fig. 23. Light propagating in a curved section of rectangular waveguide [16].